



**HAL**  
open science

## The PROMETRA Program: Fuel Cladding Mechanical Behavior under High Strain Rate

Bernard Cazalis, Jean Desquines, Christophe Poussard, Marc Petit, Yann Monerie, Christian Bernaudat, Pascal Yvon, Xavier Averty

► **To cite this version:**

Bernard Cazalis, Jean Desquines, Christophe Poussard, Marc Petit, Yann Monerie, et al.. The PROMETRA Program: Fuel Cladding Mechanical Behavior under High Strain Rate. Nuclear Technology, 2007, 157 (3), pp.215-229. 10.13182/NT07-A3814 . hal-03143868

**HAL Id: hal-03143868**

**<https://hal.science/hal-03143868v1>**

Submitted on 31 May 2022

**HAL** is a multi-disciplinary open access archive for the deposit and dissemination of scientific research documents, whether they are published or not. The documents may come from teaching and research institutions in France or abroad, or from public or private research centers.

L'archive ouverte pluridisciplinaire **HAL**, est destinée au dépôt et à la diffusion de documents scientifiques de niveau recherche, publiés ou non, émanant des établissements d'enseignement et de recherche français ou étrangers, des laboratoires publics ou privés.

# The PROMETRA Program: Fuel Cladding Mechanical Behavior under High Strain Rate

B. Cazalis<sup>a</sup>, J. Desquines<sup>a</sup>, C. Poussard<sup>b</sup>, M. Petit<sup>a</sup>,  
Y. Monerie<sup>a</sup>, C. Bernaudat<sup>c</sup>, P. Yvon<sup>b</sup>, X. Averty<sup>b</sup>

<sup>a</sup>Institut de Radioprotection et Sûreté Nucléaire, IRSN/DPAM/SEMCA, 13115 Saint-Paul lez Durance BP3, France

<sup>b</sup>Commissariat à l’Energie Atomique, CEA/DMN/SEMI, 91191 Gif-sur-Yvette, France

<sup>c</sup>Electricité de France, EDF/SEPTEN, Villeurbanne, France

An assessment of the mechanical properties of the highly irradiated fuel claddings under high strain rate has been carried out in the framework of the PROMETRA program undertaken by the French Institut de Radioprotection et de Sûreté Nucléaire in collaboration with Electricité de France and Commissariat à l’Energie Atomique (CEA). Three types of tests, including burst tests, hoop and axial tensile tests, have been performed at CEA-Saclay hot laboratories to determine the cladding tensile properties to use in the SCANAIR code. The prototypicality of each test with regard to the reactivity-initiated accident loading conditions can be addressed and analyzed in terms of strain or stress ratio. The high-strain-rate ductile mechanical properties of irradiated ZIRLO and M5 alloys derived from the PROMETRA program and their comparison to the stress-relieved irradiated Zircaloy-4 are reported. Then, the clad brittle behavior, in particular for highly corroded or spalled Zircaloy-4 cladding, is investigated.

## I. INTRODUCTION

In support of the CABRI REP-Na and CIP programs<sup>1,2</sup> performed by the French Institut de Radioprotection et de Sûreté Nucléaire (IRSN) in the framework of an international cooperation [reactivity-initiated accident (RIA) experiments in the CABRI reactor in Cadarache], the assessment of highly irradiated pressurized water reactor (PWR) cladding mechanical behavior under high strain rate has been carried out within the PROMETRA program.<sup>3-6</sup>

\*E-mail: bernard.cazalis@irsn.fr

The PROMETRA program, undertaken by IRSN in collaboration with Electricité de France (EDF) and Commissariat à l’Energie Atomique (CEA), seeks to calibrate models for Zircaloy-4, ZIRLO, and M5 hardening behavior (stress-strain curves), including effects of temperature and waterside corrosion such as oxidation and hydriding. These models derived from a large mechanical testing database gathering all the available results of tensile tests performed on ring and longitudinal samples, machined from defueled cladding between 20 and 1100°C submitted to high-strain-rate loading (0.01 to 5 s<sup>-1</sup>). Clad failure data are also investigated by means of specific tests, such as burst or plane strain tests (to be started in 2007). The models are then implemented in the SCANAIR code<sup>7,8</sup> to simulate more accurately the fuel rod behavior during a rod ejection accident (REA) in a PWR.

The first part of this paper provides an overview of the PROMETRA mechanical testing and its representativeness with regard to the RIA loading conditions.

The second part presents, compares, and discusses the ductile mechanical properties of highly irradiated Zircaloy-4 (Zry-4), ZIRLO, and M5 claddings obtained from the hoop tensile and burst tests performed at CEA-Saclay hot laboratories.

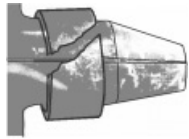
Finally, the third part of the paper reports the investigation of the clad brittle behavior, in particular for highly corroded or spalled Zry-4 cladding, by means of a specific program performed at CEA-Grenoble and pursued at CEA-Saclay.

## II. OVERVIEW OF THE PROMETRA PROGRAM

### II.A. Experimental Testing

The main types of tests performed at CEA hot laboratories are listed in Table I. The experimental procedures used for these mechanical tests have been described elsewhere.<sup>4,6</sup>

TABLE I  
PROMETRA Main Mechanical Testing

Type of Tests	Geometry	Material	Range	Objectives/Comments
CEA-Saclay axial tests		Standard Zry-4 Low-tin Zry-4	280 to 1100°C 0.01 to 5 s <sup>-1</sup>	<ul style="list-style-type: none"> <li>• Ductile behavior laws</li> <li>• Atypical failure mode</li> <li>• Joule or furnace heating</li> </ul>
CEA-Saclay hoop tensile tests		Standard Zry-4 Low-tin Zry-4 M5 ZIRLO	280 to 800°C 0.01 to 5 s <sup>-1</sup>	<ul style="list-style-type: none"> <li>• Ductile behavior laws with finite elements modeling</li> <li>• Plane stress</li> <li>• Induction heating (200°C·s<sup>-1</sup>)</li> <li>• Atypical failure mode</li> </ul>
CEA-Grenoble hoop tensile tests		Standard Zry-4	20 to 600°C → 1 s <sup>-1</sup>	<ul style="list-style-type: none"> <li>• Ductile-brittle transition</li> <li>• Failure criterion</li> </ul>
CEA-Saclay burst tests		Standard Zry-4 M5 ZIRLO	20 to 350°C 0.001 s <sup>-1</sup>	<ul style="list-style-type: none"> <li>• Failure criterion</li> <li>• Representative failure mode</li> <li>• High cost in material</li> <li>• Low temperature range</li> </ul>
CEA-Saclay Penn State tests (in progress)		Standard Zry-4 M5 ZIRLO	20 to 800°C → 1 s <sup>-1</sup>	<ul style="list-style-type: none"> <li>• Failure criterion</li> <li>• Plane strain</li> <li>• Induction heating (200°C·s<sup>-1</sup>)</li> <li>• Representative failure mode</li> </ul>

Tensile tests (axial and hoop) are mainly used to provide the clad mechanical behavior laws (stress-strain curves). In the hoop tensile test, full three-dimensional finite element analyses have been carried out with the CAST3M code<sup>9</sup> to eliminate possible artifacts due to the specimen geometry and test procedure, contact, and friction effects and to estimate local strain and stress fields. Two types of heating techniques, furnace or induction systems, are used depending on the temperature range. For temperatures higher than 480°C, the induction heating system is used to reach heating rates as high as 200°C·s<sup>-1</sup>. These high heating rates allow the prevention of any significant annealing before performing the ring tensile tests. In that case, the induction coil is located around the mandrel.<sup>10</sup>

The mechanical behavior of in-pile spalled cladding has also been addressed through a test campaign initiated at CEA-Grenoble to investigate highly corroded and spalled Zry-4 cladding and to access the ductile-brittle transition.

Moreover, in order to establish a reliable failure criterion, two other types of tests are investigated: the burst test and the plane strain test [also known as the Penn State (Pennsylvania State University) test]. The burst test is relevant for simulating a fission gas controlled

pressure loading of the cladding (second step of the RIA mechanical loading) up to failure. However, only a few burst tests have been performed at CEA-Saclay because the major concerns for this type of test are its important material consumption (due to the minimum required sample length), the difficulties of reaching high temperature levels, and keeping the strain rate constant for high-strain-rate loading. Therefore, a new test similar to the annular sample developed by Penn State<sup>11</sup> has been developed on a wider notched ring, which approaches the plane-strain conditions ( $\epsilon_{zz} = 0$ ) in its central ligament. The failure modes obtained with these notched specimens are different from those obtained on standard ring specimens.

The implementation of this test in hot cells is now under progress at CEA-Saclay. The first tests on irradiated Zry-4, ZIRLO, and M5 samples are scheduled for 2006.

## II.B. Test Matrix

The overview of the PROMETRA testing program performed on standard Zry-4 is described in Fig. 1, including the number of each type of test (valid tests only).

As can be seen, the hoop tensile tests (ring test) represent most of the tests performed on irradiated samples.

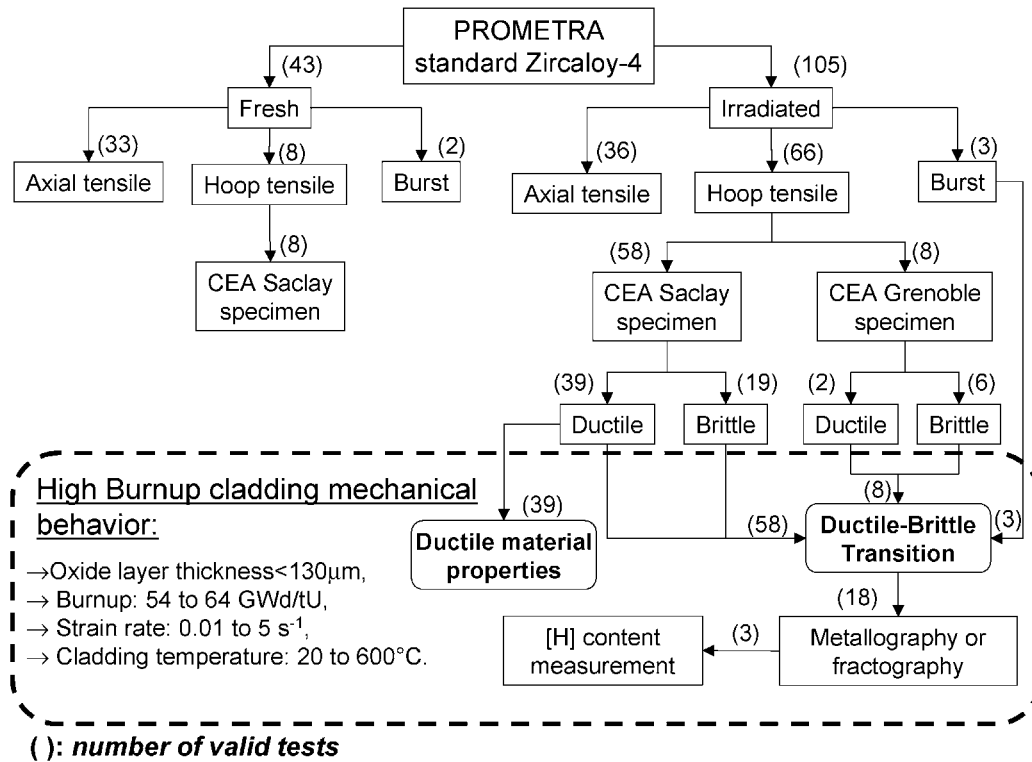


Fig. 1. Tests and analysis on standard Zry-4 performed within the PROMETRA program.

These tests provide a great amount of information but a full three-dimensional finite element analysis was required to understand the test results and ensure that this type of test could lead to a relevant material constitutive law.

More specifically, an overview of the hoop tensile tests performed on different types of irradiated cladding alloy (standard Zry-4, M5, ZIRLO) is shown in Fig. 2. All the tests performed so far on ZIRLO and M5 exhibited a ductile behavior.

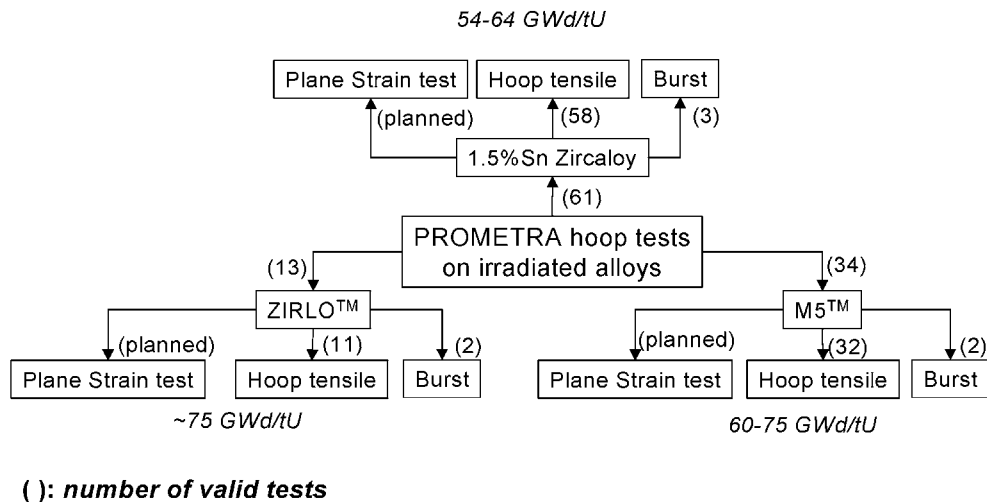


Fig. 2. PROMETRA hoop tests on irradiated cladding alloys.

## II.C. Prototypicality of Mechanical Testing for RIA Transient Analysis

First, it is important to remember that the effective fuel/clad mechanical loading during an RIA transient is not well known yet. However, tendencies can be brought out to position the domain of the applied loading. Thus, the intense fuel/clad contact pressure is at the origin of a coupling between the axial and hoop deformations, and an estimation of the ratio between hoop and axial plastic strain can be given by Eq. (1), assuming isotropic plasticity:

$$\frac{\varepsilon_{zz}^p}{\varepsilon_{\theta\theta}^p} = \frac{2 \frac{\sigma_{zz}}{\sigma_{\theta\theta}} - 1}{2 - \frac{\sigma_{zz}}{\sigma_{\theta\theta}}} \quad (1)$$

Moreover, the ratio between axial and hoop mean stresses is an increasing function of the fuel/clad friction.

The ratio of average axial strains to average hoop strains can be deduced for each CABRI REP-Na test based on posttest measurements. The average residual hoop strain is deduced from posttest profilometries, and the average residual axial strain, from residual rod elongation. Thus, the different CABRI REP-Na test plastic strain ratios can be positioned (Fig. 3) according to the stress ratio calculated with Eq. (1).

The strain ratio was considered to be a potentially influential parameter on total elongation of the specimen,<sup>12</sup> the increase of the strain ratio inducing a reduction of total elongation.

The residual strain ratio of CABRI REP-Na tests obtained with this approach varies between 0 and 1. All the tests performed on an axially short ring specimen lead, at the rupture site, to a negative axial deformation, and total elongations are overestimated when compared to RIA loading conditions. In consequence, these tests have to be interpreted by an iterative finite element analy-

sis to estimate the behavior laws in spite of the heterogeneous stress and strain fields during the test.

Similarly to the burst test, the Penn State test performed on a Penn State plane strain specimen leads to a zero plastic strain ratio. The burst test leads to high strain rate during the failure end stages, and the strain rate has for effect to decrease the ductility. Therefore, the burst test provides a lower bound of the total elongation under plane-strain displacement controlled loading.

Finally, the equal biaxial test<sup>13</sup> leads to a plastic strain ratio equal to 1. Moreover, the test results have shown that the strain to failure is similar to that obtained in the Penn State test.

We conclude that the Penn State test type appears to be representative of the low values of the deformation ratio obtained in RIA situations (0.2 to 0.6) and is expected to provide a significant improvement for fracture strain data when compared to the axially short ring tensile tests. Moreover, the orientation of the failure plane is much more typical than those obtained on ring tensile tests.

In conclusion, it has to be mentioned that the approach developed in this section is only qualitative, and its goal is not to favor one test over another or to interpret REP-Na tests but to use each of the mechanical tests in their own domain of prototypicality to provide mechanical data. As the equation used in the section does not exactly represent RIA loading conditions, it is a simple analytical approach that shows that none of the mechanical tests is fully representative of the loading, but each of them can be used for specific data. Some of these tests, as ring tensile tests, are well adapted to conventional mechanical characteristics [yield stress (YS), ultimate tensile stress (UTS), uniform elongation (UE), total elongation (TE)]. Other tests, such as burst or Penn State tests, seem better fit to failure characteristics, according to the more representative failure plane. All these data are then inserted in the SCANAIR code for RIA test simulation or interpretation.

## III. DUCTILE MECHANICAL PROPERTIES OF HIGHLY IRRADIATED ZRY-4, ZIRLO, AND M5 CLADDINGS

This section reports the main results of hoop tensile tests and burst tests performed, respectively, on ring and tube specimens machined in M5 irradiated for five and six annual cycles and in ZIRLO 75 GWd/t heavy metal (HM), and the comparison to previous results on Zry-4 irradiated for five cycles.

All the results presented in this section are related to the ductile behavior of the irradiated claddings.

### III.A. Hoop Tensile Tests Results

The investigated rods are identified in Table II. Test temperatures lie between 280 and 800°C and strain rates between 0.01/s and 5/s.

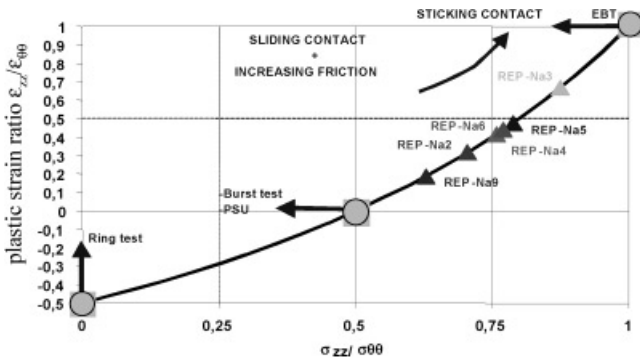


Fig. 3. Mechanical tests representativeness relative to CABRI REP-Na tests.

TABLE II  
Hoop Tensile Sample Data

Fuel Rod Cladding Type	Fuel Rod	Reactor	Rodlet Burnup (GWd/t U)	Oxide ( $\mu\text{m}$ )
ZIRLO	A12	Vandellos 2	~75	80 to 100
Five-cycle M5	Q12/4012	Gravelines 5	58	15 to 20
Six-cycle M5	N05/4021	Gravelines 5	~75	15 to 20
Five-cycle Zry-4	1055, M05, 1070 P07	Gravelines 3+2 Gravelines 3	57 to 64	15 to 130

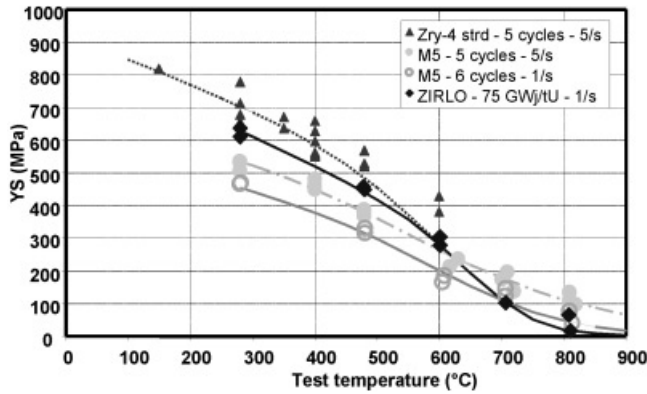


Fig. 4. Yield stress as a function of test temperature.

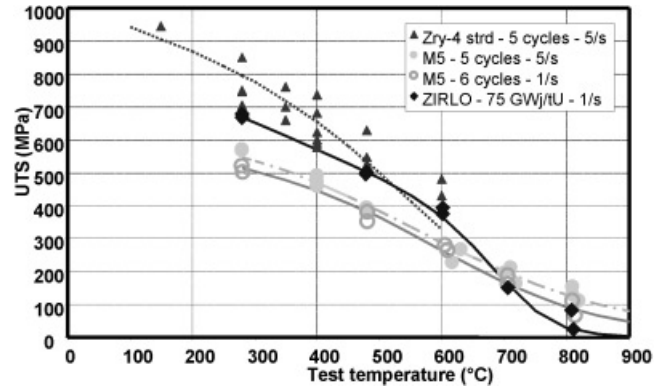


Fig. 5. Ultimate tensile stress as a function of test temperature.

In the aforementioned validity range, the ductile material strengths have been fitted according to Eq. (2) and plotted in Figs. 4 and 5:

$$Y_{s,UTS} \text{ (MPa)} = \frac{a + bT \text{ (}^\circ\text{C)}}{1 + e^{c(T \text{ (}^\circ\text{C)} - d)}} \quad (2)$$

In the case of stress-relieved Zry-4 over 600°C, fits are consistent with the results of tensile tests performed

with Joule heating. The fitted law coefficients of YS and UTS are listed in Tables III and IV, respectively.

First, it can be noted that the results observed with induction heating follow continuously the trend observed with conventional heating (furnace).

Moreover, the comparison between M5 alloy irradiated for five and six cycles and ZIRLO 75 GWd/t HM and Zry-4 alloy irradiated for five cycles indicates that for temperatures <600°C, the strengths of ZIRLO and

TABLE III  
Yield Stress Best-Fit Parameters

YS						
Material	$d\varepsilon/dt$ ( $\text{s}^{-1}$ )	a	b	c	d	Standard Deviation (MPa)
CWSR Zry-4	5	924	-0.751	0.0116	635.17	36
Five-cycle M5	5	664.9	-0.086	0.0059	553.2	15
Six-cycle M5	1	600.3	-0.472	0.0094	660.0	18
75 GWd/t U ZIRLO	1	870.0	-0.865	0.0171	681.5	21

TABLE IV  
Ultimate Tensile Stress Best-Fit Parameters

UTS						
Material	$d\varepsilon/dt$ ( $s^{-1}$ )	a	b	c	d	Standard Deviation (MPa)
CWSR Zry-4	5	1014	-0.5430	0.00803	588.6	37
Five-cycle M5	5	670.0	-0.0189	0.00584	553.7	13
Six-cycle M5	1	603.0	-0.1561	0.00744	608.6	14
75 GWd/t U ZIRLO	1	898.0	-0.8180	0.02068	705.0	25

M5 alloy (YS and UTS) are lower than those of Zry-4 alloy irradiated for five cycles. Over 600°C, the low values and the scatter of the results do not permit the establishment of a real trend. The strength differences between M5 and Zircaloy are consistent with the expected influence of the heat treatments: M5 is a recrystallized alloy and Zircaloy is a stress-relieved alloy.

A small difference between M5 irradiated five- or six-cycle strengths is noticed, but it is difficult to deconvolute the strain rate (1/s to 5/s) from the burnup effect.

The comparison between M5 alloy irradiated for five and six cycles, ZIRLO irradiated for five cycles, and Zry-4 alloy irradiated for five cycles does not show any important evolution on engineering strain up to 500°C. Uniform elongation value is  $\sim 1.5\% \pm 0.5\%$ . Over 500°C, a strain rate dependency on UE occurs (Fig. 6).

In the absence of local clip gauge, an average ductility can be estimated from the TE measured with the jack displacement. This approach may indeed lead to an apparent ductility but has to be complemented with some necking measurements. The average ductility estimated

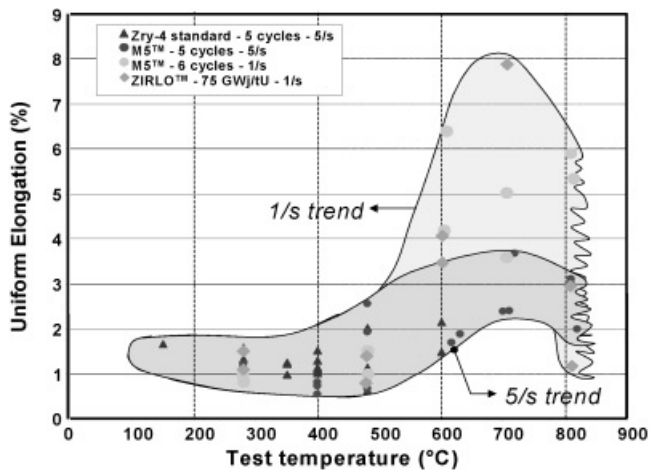


Fig. 6. Uniform elongation as a function of test temperature.

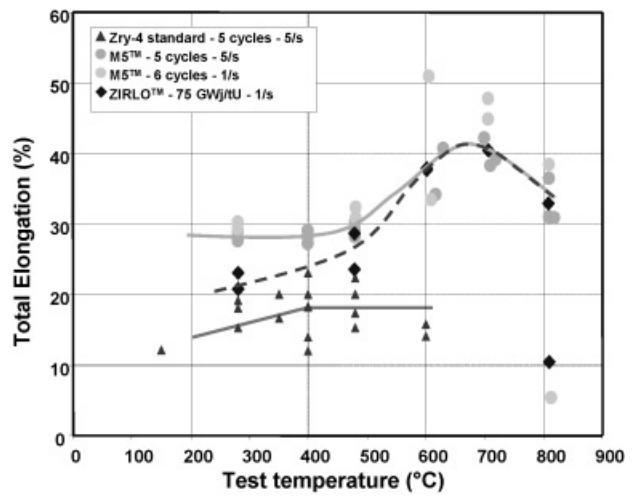


Fig. 7. Total elongation as a function of test temperature.

on the basis of the TE remains slightly higher for M5 and ZIRLO alloys than for Zry-4. A slight effect of strain rate on M5 results can be noticed over 500°C (Fig. 7).

For both alloys, one of the two samples tested near 800°C presents a very low value of TE close to the UE (5.39% compared to 5.33% in a six-cycle M5 sample).

This important apparent reduction of ductility observed in these M5 and ZIRLO specimens has been investigated by means of further posttest examinations performed at CEA-Saclay.

Figure 8 exhibits low-magnification visual examinations of the six-cycle M5 ring samples taken at different test temperatures, which show the specific nature of the ring damage near 800°C, with a very weak necking in the broken leg, giving a brittle-like appearance of the failure (Fig. 9). At the same time, the through-thickness visual examination (Fig. 10) showed a very important necking ( $\sim 80$  to 100%). Thus, the reduction of area is obtained in the width of the gauge length for temperature  $< 600^\circ\text{C}$  and through the thickness of the sample for temperatures

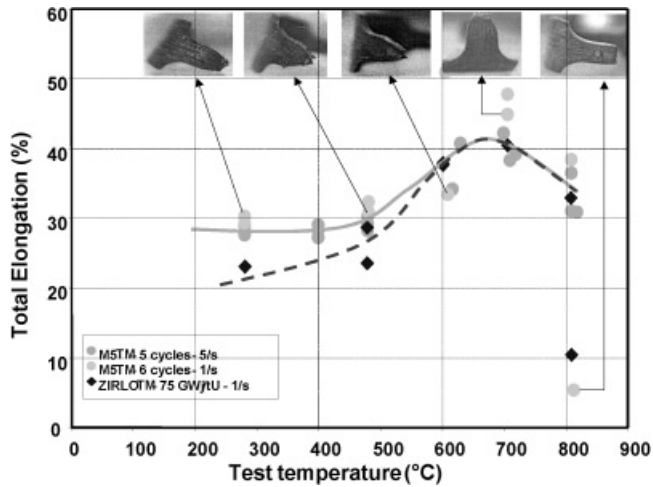


Fig. 8. M5 and ZIRLO TE as a function of test temperature with visual examinations of a six-cycle M5 sample.

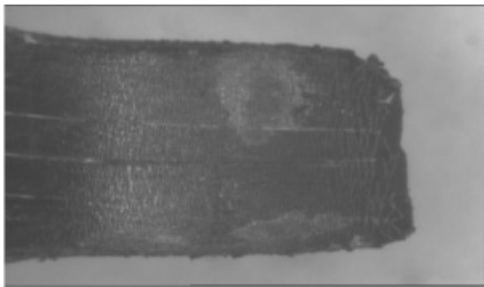


Fig. 9. Visual detail of the six-cycle M5 broken leg (ABDJ3—816°C).

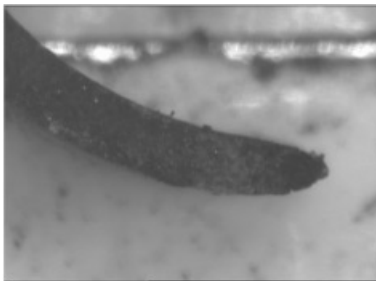


Fig. 10. Through-thickness visual detail on the six-cycle M5 sample (ABDJ3—816°C).

>600°C, which suggests that a change in the mode of deformation occurs.

Further posttest scanning electron microscopy (SEM) analyses and metallographic observations have been achieved in order to understand and explain this behavior. A total through-thickness reduction of area was con-

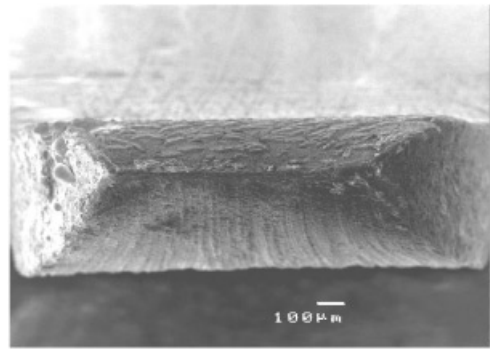


Fig. 11. SEM analysis of the six-cycle M5 broken leg (ABDJ4—809°C).

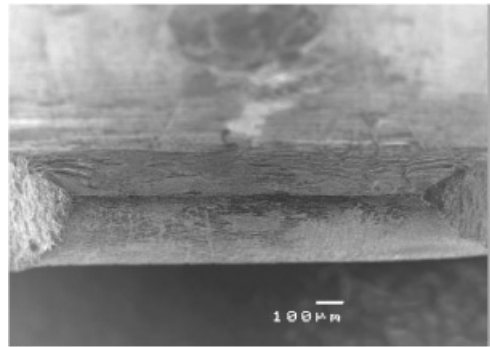


Fig. 12. SEM analysis of the ZIRLO 75 GWd/t HM broken leg (ABIO16—706°C).

firmed with the SEM analyses, as shown in Figs. 11 and 12 for both the M5 and the ZIRLO samples, respectively. For the M5, equiaxial grains (3 to 8  $\mu\text{m}$ ) with some hydrides located at the grain boundaries as well as inside the grains (Fig. 13) could be observed. In contrast to the as-received alloy, which has circumferentially oriented hydrides, they were found to be uniformly distributed without a preferential orientation after the test. For ZIRLO, a fine microstructure was observed with elongated hydrides, as shown in Fig. 14.

For both alloys, there is no evidence of an incipient phase transformation ( $\alpha \rightarrow \beta$ ). The ex-beta phase should be visible on the micrographs, if any, as a bright thin layer located preferentially at the grain boundaries. However, the present experimental methods cannot resolve low ex-beta phase contents (<10%) and especially for fast transients.

Also, different deformation mechanisms could be activated at high temperature, or the critical resolved shear stress could evolve, inducing the activation of different slip systems. These questions are under investigation.

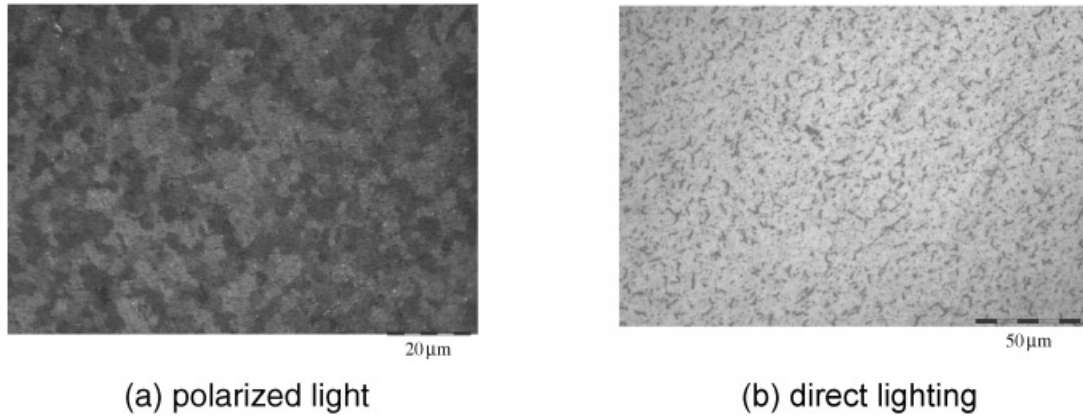


Fig. 13. Microstructure observed for the six-cycle M5 broken leg (ABDJ4—809°C).

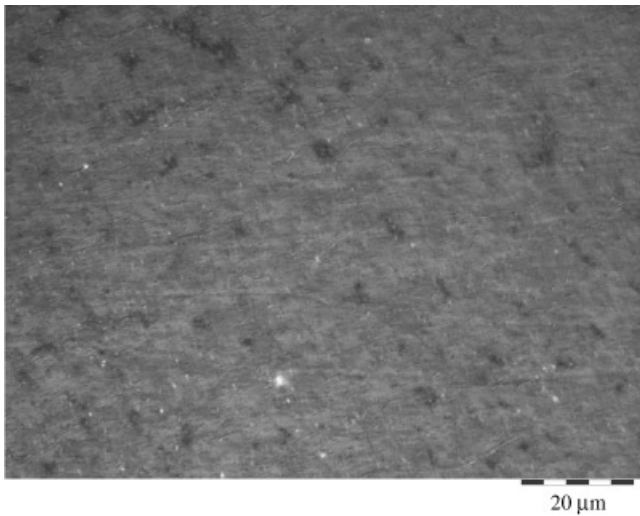


Fig. 14. Microstructure in polarized light observed for the ZIRLO 75 GWd/t HM broken leg (ABIO16—706°C).

### III.B. Burst Test Results

Burst tests on chemically defueled M5 and ZIRLO samples were performed at 280°C and at a controlled

strain rate of  $3 \times 10^{-3} \text{ s}^{-1}$ . The tested samples are presented in Table V.

During the test, the diametral deformation is monitored in situ using displacement transducers. However, as the rupture of the tube does not usually occur at the exact location of the displacement transducers, measurements only provide access to the UE. To evaluate the ductility of the material, the value of the TE has to be determined. Therefore, the hoop TE was measured from image analysis on posttest visual examination samples for ZIRLO and M5.

The results of the tests in terms of conventional mechanical characteristics (YS at 0.2% plastic strain, ultimate hoop strength, UE, TE) are presented in Table V. A quite good reproducibility of the results is obtained for both alloys.

The ZIRLO alloy shows a mean strength of 690 MPa to be compared to 622 MPa for the M5 alloy. The experimental results show a fairly low hoop UE (0.5 to 0.6%) for both alloys.

Figures 15 and 16 show the samples after burst tests. These pictures reveal that the clad deformation is more pronounced for the M5 alloy than for the ZIRLO alloy: The M5 alloy shows a large ballooning and short axial crack (the crack length is  $\sim 9$  mm for a maximum

TABLE V  
Description and Main Results of Burst Tests

Fuel Rod Cladding Type	Fuel Rod	Reactor	Rodlet Burnup (GWd/t U)	Sample Identity	Oxide ( $\mu\text{m}$ )	Temperature ( $^{\circ}\text{C}$ )	YS (MPa)	UTS (MPa)	UE (%)	TE (%)
ZIRLO	A06	Vandellos 2	$\sim 75$	DFLE	94	280	657	692	0.49	0.50
				DFIM	88	281	654	688	0.55	2.7
M5	4034	Gravelines 5	$\sim 75$	ABEF	16	281	604	625	0.51	12.2
				ABEJ	17	281	597	619	0.62	16.2

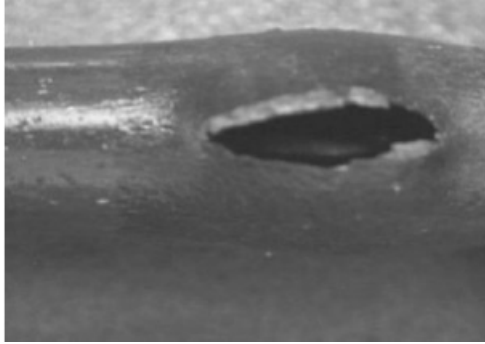


Fig. 15. Burst test on M5 sample (ABEF).



Fig. 16. Burst test on ZIRLO sample (DFIM).

pressure of 87.6 MPa at ultimate hoop strength), indicating a high ductility, with an average total hoop elongation of 14%.

For the ZIRLO samples, the crack is elongated and straight. Zirconia spalling occurs in the vicinity of the cracks. Lower total hoop elongations are measured (1.6% on average, which is close to the hoop UE considering the accuracy of 2%). The crack length reaches 18 mm for a maximum pressure of 82.6 MPa at ultimate hoop strength.

This difference of ductility between both alloys is explained by the well-known influence of the material corrosion, higher for the ZIRLO alloy than for the M5 alloy.

#### IV. INVESTIGATION OF THE BRITTLE BEHAVIOR OF HIGH-BURNUP STRESS-RELIEVED ZRY-4 CLADDING

##### IV.A. Overview of the PROMETRA Testing on Highly Corroded Spalled Claddings

The case of clad brittle behavior, in particular for highly corroded or spalled cladding, deserves a different

treatment. Thus, the investigation of the ductile-brittle transition has been performed by means of a specific program consisting mainly in two special series of hoop tensile tests performed in CEA laboratories:

1. a first series (see Table VI), carried out by CEA-Grenoble on mechanically defueled plain rings (i.e., without any thinner section); the specimens are spalled samples stemming from span 6 of the QO2 rod used for REP-Na 1 ( $ZrO_2 \approx 85 \mu m$ ) (see Table VII)
2. a second series (see Table VIII), carried out by CEA-Saclay on machined samples, ring specimen of spalled cladding stem from span 5 of the M05 rod (sibling rod of REP-Na 1 parent rod), and from span 6 of the P07 rod used for REP-Na 8 ( $ZrO_2 \approx 110$  to  $130 \mu m$ ) (see Table VII).

The failure mode, especially brittle failure with cracks orthogonal to the main loading direction, is best determined from the posttest appearance of the specimen as seen globally by visual examination and locally by optical microscopy or by SEM. Moreover, analysis of the

TABLE VI

CEA Grenoble Hoop Tensile Test Results Obtained for an Intensively Spalled Cladding

Specimen <sup>a</sup>	Oxide Thickness ( $\mu m$ )	Hydrogen Content (ppm)	Strain Rate ( $s^{-1}$ )	Testing Temperature ( $^{\circ}C$ )	TE (%)	UTS (MPa)
Q02-555	74	603 <sup>b</sup>	0.01	350	0	401
Q02-557	75	610 <sup>b</sup>	5	350	2	469
Q02-558	76	618 <sup>b</sup>	0.01	350	0	418
Q02-560	86	573	0.01	280	12	624
Q02-562	79	1882	5	280	0.05	450
Q02-563	85	1621	0.01	280	1.5	586
Q02-565	82	665 <sup>b</sup>	0.01	350	8	554
Q02-566	80	645 <sup>b</sup>	0.01	350	1.5	568

<sup>a</sup>Extracted from REP-Na 1 parent rod, QO2, span 6, with an average burnup of 63.4 MWd/kg U, irradiated in Gravelines 3+2 EDF reactor ( $17 \times 17$  PWR), stress-relieved Zry-4.

<sup>b</sup>Deduced from a correlation between the average oxide thickness and the hydrogen content.

TABLE VII  
Fuel Rod Data

Rod	Irradiated Site	Average Burnup (MWd/t U)	Fuel	Comment
M05	Gravelines 3+2	60 278	UO <sub>2</sub>	Q02 (REP-Na 1) twin rod
P07	Gravelines 3+2	54 700	UO <sub>2</sub>	REP-Na 8 parent rod

TABLE VIII  
CEA-Saclay Hoop Tensile Tests on Highly Corroded Spalled Claddings Supported by Fractography or Metallography

Specimen	Parent Rod/Span	Oxide Thickness ( $\mu\text{m}$ )	Hydrogen Content (ppm)	Strain Rate ( $\text{s}^{-1}$ )	Testing Temperature ( $^{\circ}\text{C}$ )	TE (%)	UTS (MPa)
2400	M05/5	90	727 <sup>a</sup>	0.01	280	2.3	650
2401	M05/5	90	727 <sup>a</sup>	0.2	400	3.2	618
2402	M05/5	90	727 <sup>a</sup>	0.2	400	15.0	578
2403	M05/5	90	727 <sup>a</sup>	5	280	15.3	704
2404	M05/5	90	727 <sup>a</sup>	5	400	18.2	600
2405	M05/5	90	727 <sup>a</sup>	5	400	1.7	618
2468	P07/6	130	1038 <sup>a</sup>	5	480	0.0	$\sim 145^{\text{b}}$
2470	P07/6	130	1038 <sup>a</sup>	0.01	280	0.6	617
2472	P07/6	130	1038 <sup>a</sup>	5	280	7.1	702

<sup>a</sup>Deduced from a correlation between the average oxide thickness and the hydrogen content.

<sup>b</sup>Out-of-gauge section failure, UTS approximately corrected.

information deduced from the fractographies and metallographies of the CEA-Saclay ring specimen allows one to determine parameters, such as the initiated crack depth, characterizing the clad embrittlement.

#### IV.B. Analysis of Hydride-Related Embrittlement in Oxide-Spalled Cladding

It has been observed on high-burnup fuel cladding that applying very similar loading conditions to apparently similar claddings led to very different test results. To illustrate this statement, a set of load-displacement curves obtained on three CEA-Saclay hoop tensile tests are plotted in Fig. 17. The three tests have comparable outer oxide layer depth (130  $\mu\text{m}$ ). Oxide layers of tests 2462 and 2463 were subjected to in-pile spallation, and the gauge section was machined in a spalled area and the oxide layer of test 2471 remained unspalled. The behavior of test 2471 is ductile, whereas the behavior of tests 2462 and 2463 is clearly brittle.

The usual signs of cladding embrittlement on axially short hoop tensile ring tests are

1. unusually low fracture strain
2. fracture plane not oriented at 45 deg but in a radial-axial direction.

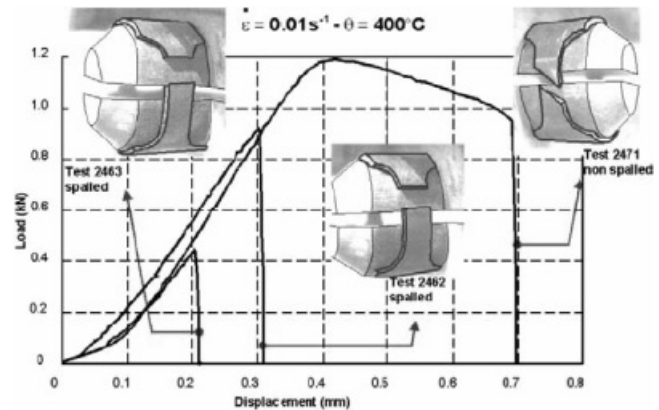
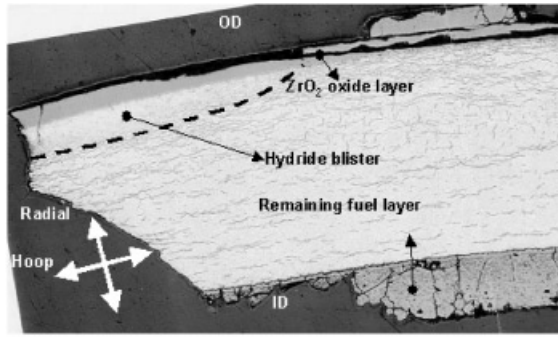


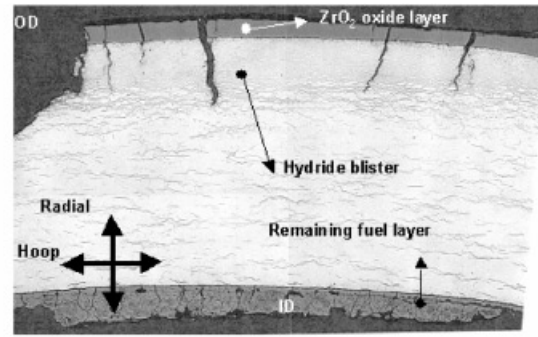
Fig. 17. Cladding embrittlement on CEA-Saclay hoop tensile test at 400°C and 0.01/s .

##### IV.B.1. Metallographic Aspect of Hydride Embrittlement

The brittle behavior of highly corroded, stress-relieved Zry-4 claddings has been related to hydride embrittlement in the PROMETRA program. Two main kinds of hydride damages have been evidenced:



Q02-557 CEA -Grenoble hoop tensile test



Q02-566 CEA -Grenoble hoop tensile test

Fig. 18. Hydride blisters on posttest metallography after hydride etching.

1. hydride blisters illustrated in Fig. 18
2. hydride rims illustrated in Fig. 19.

In the framework of the PROMETRA program, for stress-relieved Zry-4, pure zirconium hydrides with lenticular shape, called hydride blisters or hydride lenses, have been frequently observed, but only on spalled claddings. The usually invoked mechanism (see Ref. 14, for example) to generate these hydride lenses is that in the spalled area of a highly corroded cladding, there is a cold spot attracting the hydrogen dissolved in the surrounding hot area by a diffusion mechanism. This mechanism is the one used to create artificial hydride blisters in Zircaloy.<sup>15</sup>

Hydride-rich rims sometimes appear at the outer diameter of the cladding at a pellet/pellet interface. The colder region surrounding this interface also attracts hydrogen, enhancing cladding corrosion.<sup>16</sup> Thus, there is also usually a thicker corrosion layer at pellet/pellet interfaces.<sup>14</sup> This mechanism corresponds to axially short hydride rims. Axially extensive hydride rims are also sometimes observed on fractographic examinations after

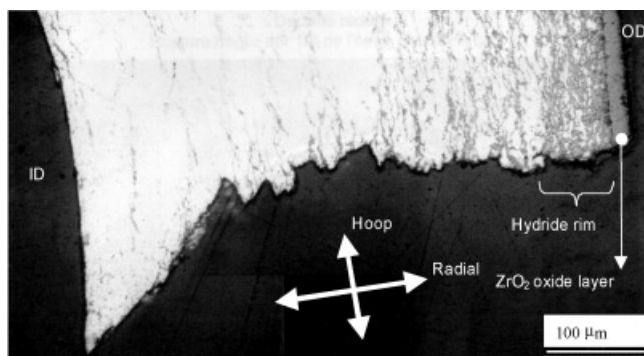


Fig. 19. Hydride rim on posttest metallography of CEA-Saclay hoop tensile test 2470 after hydride etching (70- $\mu\text{m}$ -deep hydride rim).

burst tests; axial extensions of 100  $\mu\text{m}$  are not unusual. The high corrosion level and the colder outer diameter might alone explain the generation of such extended hydride rims, which are observed not only on spalled claddings but also on highly corroded, unspalled claddings. The inner diameter region is always hot and usually hydride depleted (thermally driven hydrogen diffusion toward the cold regions). A very tiny hydride rim is sometimes observed close to the inner diameter wall; this can be linked to the presence of the inner diameter wall zirconium oxide layer.

The hydride-induced embrittlement is exacerbated by oxide-layer spallation during in-reactor operation, but it is sometimes observed on very oxidized cladding samples without any spallation. This result is consistent with previous studies.<sup>14</sup>

#### IV.B.2. Fractographic Aspect of Hydride Embrittlement

Before identifying hydride embrittlement fingerprints on SEM observations, it is necessary to establish the reference fracture aspect of a ductile failure.

Figures 20 and 21 present the usual posttest fractographic aspect of a ductile specimen (PROMETRA 2403, on the M05 rod span 5). A low-magnification SEM image is shown in Fig. 20. In this figure, the failure plane is orientated at 45 deg to the loading direction; this is one of the macroscopic indications of a ductile failure. Some necking can be observed in Fig. 20c; here, four locations are indicated and high-magnification SEM examinations of each of these locations appear in Fig. 21.

In Fig. 21, the fracture aspect is fully transgranular with ductile dimples at all locations. Figure 21c shows the onset of ductile failure; microvoid coalescence nucleated a penny-shaped crack in the middle of the specimen. This crack failed in a ductile manner in a highly porous (many microvoids nucleated) material.

The SEM observations performed on CEA-Saclay hoop tensile test 2400 (Table VII) are shown in Fig. 22. The fracture aspect is typical of a specimen with a

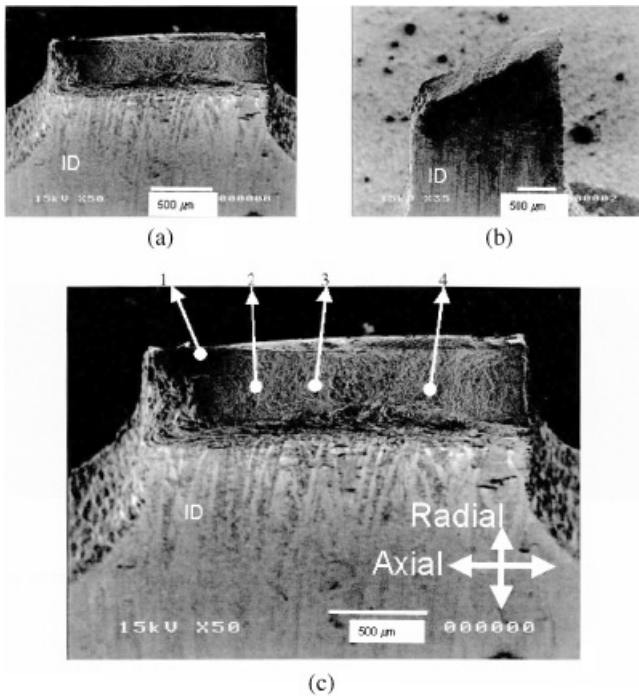


Fig. 20. Low-magnification aspect of ductile failure in PROMETRA test 2403.

hydride rim located at the outer diameter. The outer region with a pseudocleavage fracture aspect is included in a radial-axial plane; the inner region with ductile dimples has a 45-deg orientation. The main fracture steps identified in Refs. 17 and 18 can also be derived from this fractography. An incipient crack is initiated in the hydride rim, the crack being in a radial axial plane. There is a potential for radial crack growth and for a sufficiently high tensile stress or strain so that the remaining ligament cannot carry the load anymore and the specimen fails with a 45-deg rotated fracture angle.

The lessons learned from the PROMETRA fractographic examinations can be summarized as follows.

The fingerprint of a brittle failure caused by a hydride blister is

1. cleavage in the outer-diameter wall at the blister location (in an axial radial fracture plane)
2. potentially pseudocleavage surrounding this area (in the same axial radial fracture plane)
3. ductile dimples and failure plane change, out of the brittle area (in a 45-deg rotated fracture plane).

The fingerprint of a brittle failure caused by an outer-diameter-located hydride rim is

1. pseudocleavage in the hydride-rich rim (in an axial radial fracture plane)

2. ductile dimples and failure plane change, out of the brittle area (in a 45-deg-rotated fracture plane).

#### IV.B.3. Size of Hydride Damage

The observed depth of hydride lenses ranged from nearly zero up to the entire cladding thickness. In the case of PROMETRA test 2468, performed on the highly corroded P07 rod with 130- $\mu\text{m}$  oxide layer thickness and oxide spallation, a through-wall hydride lens has been evidenced and is illustrated in Fig. 23. This specimen failed out of the gauge section, and a rough estimate of the failure stress,  $\sim 145$  MPa, could be determined. It is the lowest failure stress measured within the entire PROMETRA database on high-burnup stress-relieved Zry-4. Very low failure stress values were also obtained on some other ring tests or burst tests that failed at higher but similar stress levels.

It is assumed that 145 MPa is approximately the fracture hoop stress of a hydride blister. This value has the same order of magnitude as the one determined in Ref. 17 on fresh cladding with laboratory-created blisters.

#### IV.B.4. Analysis of the Influence of Hydride Damage Depth on Sample Integrity

The hydride damage depth, defined as the hydride blister depth or hydride rim depth, has been roughly estimated either from metallography (based on hydride etching) or from fractography (pseudocleavage-affected depth) of specimens tested between 280 and 480°C. The obtained hydride damage depth values normalized by the sound cladding thickness are presented in Fig. 24. In this figure, two curves are plotted: the normalized fracture stresses and the normalized plastic strains at failure (actually residual strains divided by ductile TE value at the corresponding temperature), as derived from these post-test examinations.

Figure 24 illustrates the deleterious influence of hydride damage on cladding mechanical properties. For a hydride damage deeper than 30 to 40% of the sound cladding thickness, no residual strain is expected. Similar curves were obtained on fresh Zircaloy with hydride rims or hydride blisters reported in Refs. 18 and 19 and more recently in Ref. 17. The fracture strain, determined mainly on ring specimens with near-uniaxial tension loading, most probably overpredicts the integrity of an actual irradiated fuel rod submitted to RIA loading under close-to-plane strain loading conditions.<sup>20</sup>

## V. CONCLUSIONS

Transient mechanical properties of high-burnup PWR claddings have been investigated through the PROMETRA program.

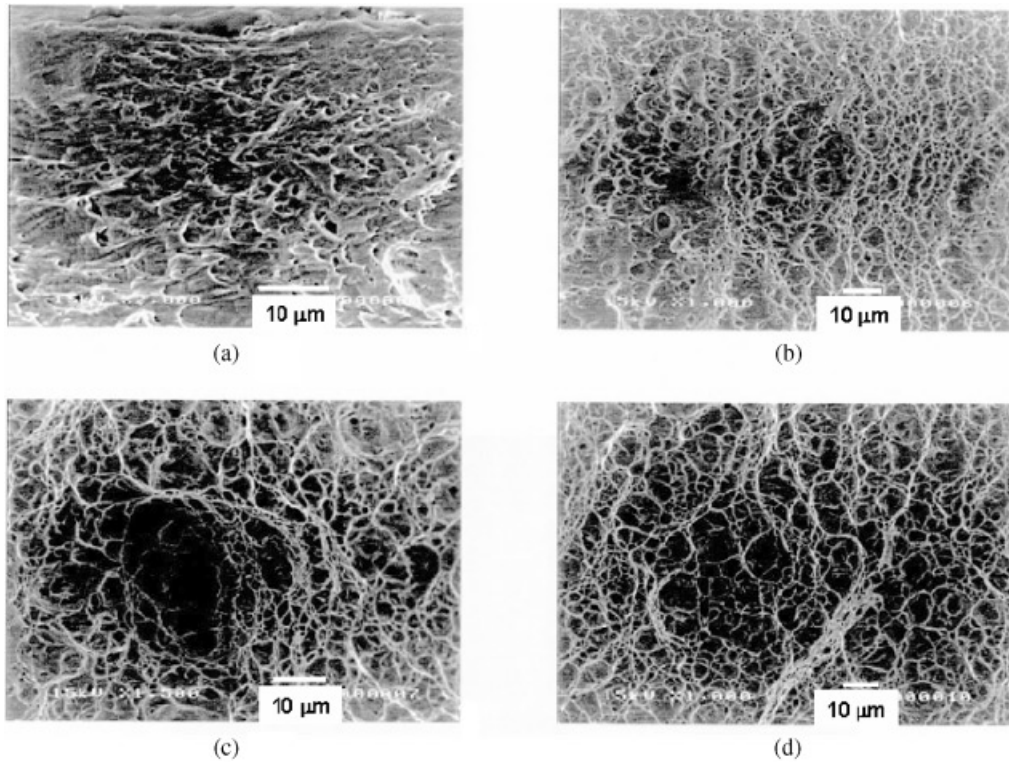


Fig. 21. High-magnification aspect of ductile failure in PROMETRA test 2403.

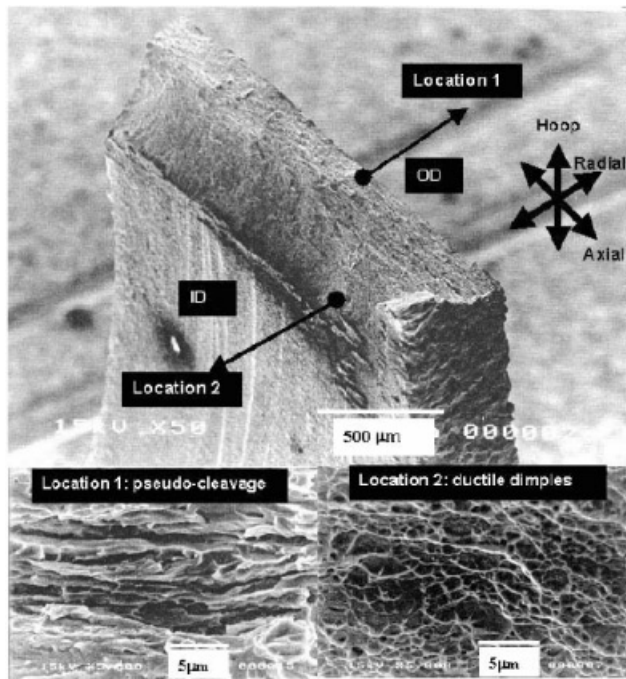


Fig. 22. Brittle failure initiated by a hydride rim on PROMETRA test specimen 2400.

The representativeness of each test with regard to the RIA loading conditions has been addressed and analyzed. Thus, the Penn State test, scheduled in CEA-Saclay hot laboratories, appears to be representative of the low values of the strain ratio obtained in an RIA situation and is expected to provide a significant improvement of the rupture criterion when compared to the axial short-ring tensile tests.

A material database, including all the available results of burst and tensile tests on high-burnup stress-relieved Zry-4, ZIRLO, and M5 alloy, has been developed and now released. Detailed three-dimensional finite element analyses have been achieved to understand the tests results and validate the geometries. All the ductile parameters deduced from PROMETRA are expected to be valid for burnups higher than  $\sim 30$  GWd/tU up to 60 GWd/t for Zry-4 and 75 GWd/tU for ZIRLO and M5, and for temperatures up to 800°C obtained with the induction heating device.

The ductility of ZIRLO and M5 cladding is clearly higher than that of Zry-4 cladding up to 600°C. Over 600°C, some tested samples exhibit an important reduction of ductility, not fully understood at this time.

For spalled claddings, most of the generated results converge to demonstrate that the failure conditions are

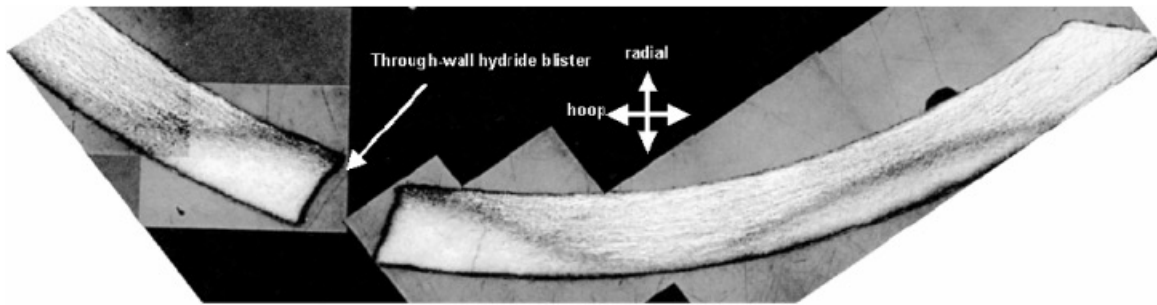


Fig. 23. Metallography with hydride etching of the brittle PROMETRA test 2468.

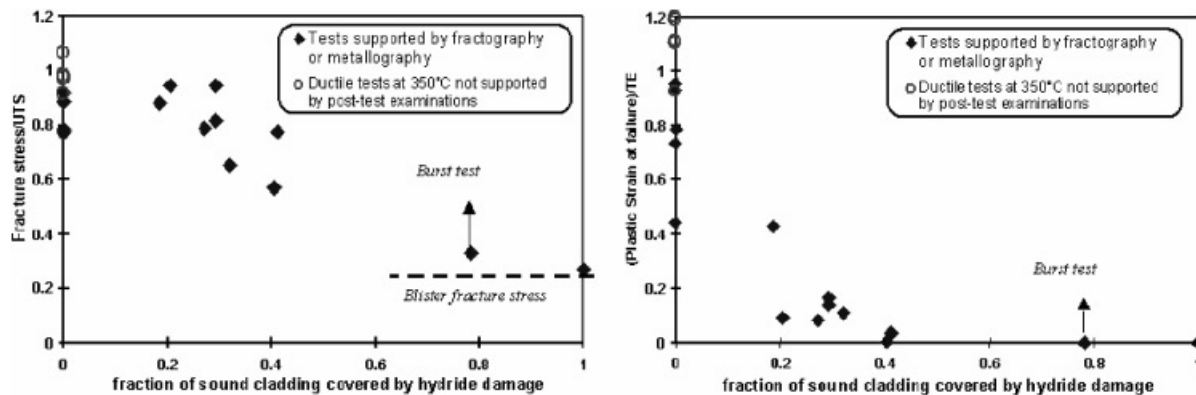


Fig. 24. Influence of hydride damage depth on fracture stress and fracture strain.

difficult to predict. Potentially very deep hydride blisters and hydride rims have been observed on some of the specimens having a spalled outer zirconia layer using fractography or metallography. For thick oxide layers without spallation, only hydride rims have been evidenced on the outer diameter of the cladding using metallography. There is no direct link between oxide layer thickness or spallation state and hydride damage depth (hydride blister depth or hydride rim depth). The fracture conditions strongly depend on hydride content and distribution. There is no evidence of specific embrittlement at the inner diameter within all metallographic examinations.

The new investigations of the PROMETRA program focus on new experimental techniques (clad rupture acoustic detection, image analysis, biaxial testing, etc.) and materials of present and future interest, including ZIRLO, M5, and boiling water reactor claddings.

#### ACKNOWLEDGMENTS

The contribution of C. Duguay, O. Rabouille, P. Bottin, J. P. Pizzanelli, S. Allegre, and J. J. Espinas, research engineers

and technicians at CEA-Saclay, is gratefully acknowledged. Moreover, the authors would like to thank H. S. Rosenbaum, who substantially contributed to better understanding the data generated within the PROMETRA program.

#### REFERENCES

1. J. PAPIN, B. CAZALIS, J. M. FRIZONNET, J. DES-QUINES, F. LEMOINE, V. GEORGENTHUM, F. LAMARE, and M. PETIT, "Summary and Interpretation of the CABRI REP-Na Program," *Nucl. Technol.*, **157**, 230 (2007).
2. J. PAPIN, C. LECOMTE, and J. C. MELIS, "Definition and Status of the CABRI International Program for High Burnup Fuel Studies," *Proc. 28th WRSW*, Bethesda, Maryland, October 23–25, 2000 (2000).
3. M. BALOURDET, C. BERNAUDAT, V. BASINI, and N. HOURDEQUIN, "The PROMETRA Programme: Assessment of Mechanical Properties of Zircaloy 4 Fuel Properties During an RIA," *Trans. 15th Int. Conf. Structural Mechanics in Reactor Technology (SMiRT-15)*, Seoul, Korea, August 15–20, 1999, p. II-485 (1999).

4. P. YVON, C. SAINTE CATHERINE, C. DUGUAY, S. CARASSOU, N. HOURDEQUIN, B. CAZALIS, and C. BERNAUDAT, "Development of New Techniques to Assess the Mechanical Behaviour of Zircaloy-4 During an RIA," presented at IAEA Technical Committee Mtg. Fuel Behavior Under Transient LOCA Conditions, Halden, Norway, September 10–14, 2001.
5. B. CAZALIS, J. DESQUINES, C. BERNAUDAT, C. POUSSARD, X. AVERTY, and P. YVON, "The PROMETRA Program: A Reliable Material Database for Highly Irradiated Zircaloy-4, Zirlo, M5 Fuel Claddings," *Proc. SMIRT-18*, Beijing, China, August 7–12, 2005 (2005).
6. J. DESQUINES, B. CAZALIS, C. BERNAUDAT, C. POUSSARD, X. AVERTY, and P. YVON, "Zircaloy-4 Fuel Cladding Mechanical Behavior in the Field of RIA Transients Through the PROMETRA Program," *Proc. Conf. Zirconium in the Nuclear Industry*, Stockholm, Sweden, June 2004, American Society for Testing and Materials (2004).
7. E. FEDERICI, F. LAMARE, V. BESSIRON, and J. PAPIN, "Status of Development of the SCANAIR Code for the Description of Fuel Behavior Under Reactivity Initiated Accidents," presented at Int. Topl. Mtg. Light Water Reactor Fuel Performance, Park City, Utah, April 10–13, 2000.
8. E. FEDERICI, F. LAMARE, V. BESSIRON, and J. PAPIN, "The SCANAIR Code Version 3.2: Main Features and Status of Qualifications," presented at IAEA Technical Committee Mtg. Fuel Behavior Under Transient LOCA Conditions, Halden, Norway, September 10–14, 2001.
9. CAST3M, CEA Saclay Finite Element Code, available on the Internet at <http://www-cast3m.cea.fr/cast3m>
10. X. AVERTY, P. YVON, C. DUGUAY, J. P. PIZZANELLI, and V. BASINI, "Induction Heating on Dynamic Tensile Tests in CEA Saclay," *Proc. 39th Mtg. European Hotlabs at CIE-MAT*, Madrid, Spain, October 22–24, 2001, p. 39 (2001).
11. T. M. LINK, D. A. KOSS, and A. T. MOTTA, "Failure of Zircaloy Cladding Under Transverse Plane-Strain Deformation," *Nucl. Eng. Des.*, **186**, 379 (1998).
12. F. YUNCHANG and D. A. KOSS, "The Influence of Multi-axial States of Stress on the Hydrogen Embrittlement of Zirconium Alloy Sheet," *Metal. Trans. A*, **16**, 675 (1985).
13. A. GLENDENING, D. A. KOSS, A. T. MOTTA, O. N. PIERRON, and R. S. DAUM, "The Influence of Strain State on the Failure of Hydrided Zircaloy-4," *Proc. Conf. Zirconium in the Nuclear Industry*, Stockholm, Sweden, June 2004, American Society for Testing and Materials (2004).
14. A. M. GARDE, G. P. SMITH, and R. C. PIREK, "Effects of Hydride Precipitate Localization and Neutron Fluence on the Ductility of Irradiated Zircaloy-4," *Proc. 11th Int. Symp. Zirconium in the Nuclear Industry*, ASTM STP 1295, p. 407, E. R. BRADLEY and G. P. SABOL, Eds., American Society for Testing and Materials (1996).
15. G. DOMMIZZI, R. A. ENRIQUE, J. OVEJERO-GARCIA, and G. C. BUSCAGLIA, "Blister Growth in Zirconium Alloys: Experimentation and Modeling," *J. Nucl. Mater.*, **229**, 36 (1996).
16. M. BLAT and D. NOEL, "Detrimental Role of Hydrogen on the Corrosion Rate of Zirconium Alloys," *Proc. 11th Int. Symp. Zirconium in the Nuclear Industry*, ASTM STP 1295, p. 319, E. R. BRADLEY and G. P. SABOL, Eds., American Society for Testing and Materials (1996).
17. O. N. PIERRON, D. A. KOSS, A. T. MOTTA, and K. S. CHAN, "The Influence of Hydride Blisters on the Fracture of Zircaloy-4," *J. Nucl. Mater.*, **322**, 21 (2003).
18. R. S. DAUM, S. MAJUMDAR, D. W. BATES, A. T. MOTTA, D. A. KOSS, and M. C. BILLONE, "On the Embrittlement of Zircaloy-4 Under RIA-Relevant Conditions," *Proc. 13th Int. Symp. Zirconium in the Nuclear Industry*, ASTM STP 1423, p. 702, G. D. MOAN and P. RUDLING, Eds., West Conshohocken, Pennsylvania, 2002, American Society for Testing and Materials (2002).
19. D. W. BATES, "Influence of Stress State and Hydrogen on Deformation and Failure of Zircaloy-4," Thesis, Nuclear Engineering, The Pennsylvania State University (1998).
20. F. YUNCHANG and D. A. KOSS, "The Influence of Multi-axial State of Stress on the Hydrogen Embrittlement of Zirconium Alloy Sheet," *Metal. Trans. A*, **16**, 675 (1985).